

Systematic search for cool hypervelocity stars in multi-epoch WISE data

S. Karpov¹, O. Malkov², and A. Avdeeva²

¹ Institute of Physics, Czech Acad. Sci., 182 21 Prague 8, Czech Republic e-mail: karpov@fzu.cz

² Institute of Astronomy, 48 Pyatnitskaya St., Moscow 119017, Russia

Received September 15, 1996; accepted March 16, 1997

ABSTRACT

Context. Sixty years after the discovery of brown dwarfs, the search for these objects continues, particularly in the vicinity of the Sun. Objects near the Sun are characterized by large proper motions, making them seen as fast-moving objects. While the Gaia DR3 catalogue is a comprehensive source of proper motions, it lacks the depth needed for discovering fainter objects. Modern multi-epoch surveys, with their greater depth, offer a new opportunity for systematic search for ultra-cool dwarfs.

Aims. The study aims to systematically search for high proper motion objects using the newly released catalogue of epochal WISE data in order to identify new brown dwarf candidates in the solar neighborhood, estimate their spectral types, distances and spatial velocities.

Methods. We used recently released unTimely catalogue of epochal detections in unWISE coadds to search for objects with high proper motions using simple motion detection algorithm. This method was used to identify objects with proper motions exceeding approximately 0.6 arcseconds per year. The identified objects were then cross-referenced with data from other large-scale sky surveys to further analyze their characteristics.

Results. The search yielded 3245 moving objects with significant proper motions, 32 of which had not been previously published. Among these, at least 15 were identified as reliable new brown dwarf candidates, with estimated distances closer than 50 parsecs and spectral types later than T0.

Key words. brown dwarfs – proper motions – surveys

1. Introduction

Brown dwarfs are substellar objects with masses insufficient to start and maintain stable hydrogen fusion, which causes them to cool over time. They were theoretically predicted (Kumar 1963; Hayashi & Nakano 1963) and then later discovered (Rebolo et al. 1995; Nakajima et al. 1995). Since then, the search for new brown dwarfs, and systematic study of known ones is a major problem in stellar astrophysics.

According to recent studies (Mužić et al. 2017), the number of brown dwarfs in the Galaxy ranges from 25 to 100 billion objects (with the total number of objects ranging from 100 to 500 billion). Homogeneous and complete samples of brown dwarfs are needed for various kinds of studies: kinematic studies (Smith et al. 2014), studies of binary stars with brown dwarfs (Lodieu et al. 2014), and studies of the parameters of the Galaxy.

The search for brown dwarfs has evolved significantly over the years, building upon techniques initially developed for finding late-type M dwarfs in photographic surveys. Among these, photometric selection has emerged as the dominant strategy for searching for brown dwarfs in wide-field surveys. The method's effectiveness relies on the key difference in spectral characteristics between the target objects and the majority of the background population. This distinction allows one to identify the specific region of color space that characterises primary brown dwarf population.

The searches based on color selection method and characterisation of brown dwarfs were performed using DENIS (Delfosse et al. 1997; Phan-Bao et al. 2008), 2MASS (Kirkpatrick et al.

1999), SDSS (Fan et al. 2000; Chiu et al. 2006), UKIDSS (Day-Jones et al. 2013; Burningham et al. 2013), CFDBS (Delorme et al. 2008), WISE (Kirkpatrick et al. 2011) and most recently DES (Carnero Rosell et al. 2019; dal Ponte et al. 2023) surveys. In many cases, cross-matching different catalogues are useful. For example, the 2MASS passbands alone are not sufficient to distinguish from stars of other classes, although they help in classifying between subclasses of brown dwarfs. Furthermore, by combining optical data from Pan-STARRS with WISE data, researchers have successfully targeted LT transition objects that are typically hard to detect in near-infrared surveys (Best et al. 2015, 2018).

Such selection, however, was rarely perfect, even with a combination of a number of surveys. Photometric samples are often contaminated with extraneous objects, requiring spectroscopic confirmation to establish reliable samples. The only search for brown dwarfs based on spectra was conducted by (Schmidt et al. 2010). The work utilised SDSS DR7 spectroscopic database and provided 210 newly discovered brown dwarfs, showing that the existing color selection method are biased towards redder brown dwarfs.

As brown dwarfs are very faint and therefore only can be found close to the Sun, their proper motions should be large, compared to the majority of the field stars. Combined with typically suboptimal angular resolution of infrared instruments, it significantly complicates the association of measurements between different datasets acquired at different epochs, leading to predominantly slower moving objects being detected using color selection methods.

To overcome this bias, uniform data sets with dense multi-epoch coverage are needed. The multi-epoch data from 2MASS survey (Kirkpatrick et al. 2010) and from AllWISE Motion Survey (Kirkpatrick et al. 2014) with a spectroscopic follow-up have revealed previously unknown LT dwarfs and subdwarfs. The large-scale search for rapidly moving brown dwarfs is nowadays enabled by the CatWISE (Marocco et al. 2021) catalogue that reports both infrared color and proper motions for nearly two billions of objects over the whole sky. However, as the object detection in CatWISE is performed on the co-added images combining all unWISE epochs, it is not optimal for finding rapidly moving stars, and prone to numerous spurious detections due to aggressive deblending applied to the data. Thus, the projects like Backyard Worlds have to utilize citizen science approach for visual inspection of many candidate sources in order to find actual moving objects (Kuchner et al. 2017; Rothermich et al. 2024; Marocco et al. 2024).

On the other hand, recent release of unTimely Meisner et al. (2023) catalogue of epochal detections in individual unWISE coadds opens the possibility of direct search for most rapidly moving objects. Here we describe such a search that we performed on W2 band data in order to specifically find new candidates for nearby cool dwarfs. In Section 2 we describe the algorithm and data we used, as well as the moving objects we detected. Section 3 contains the discussion of the sensitivity of our search, presents the list of high proper motion objects we detected that lack both Gaia detections and Simbad records, and reviews their properties and possible classification as late-type cool dwarf candidates. Finally, Section 4 concludes the work.

2. Data and analysis

The Wide-field Infrared Survey Explorer, or WISE (Wright et al. 2010), is a space telescope that performed all-sky survey initially in four infrared bands (W1 at $3.4\mu\text{m}$, W2 at $4.6\mu\text{m}$, W3 at $12\mu\text{m}$ and W4 at $22\mu\text{m}$), and since the coolant depletion in late 2010 – in two shorter-wavelengths bands only. It repeatedly scanned the sky in great circles near a solar elongation of 90° , typically observing a given region of the sky over a period of 1 d every 6 months, with denser coverage closer to the ecliptic poles. unWISE coadds combine the exposures from the same sky regions into a series of six-monthly visits, with an average of typical 12 exposures per band per visit (Meisner et al. 2019, 2018). These coadds are both sharper and deeper than original data used for producing initial AllWISE catalogue (Cutri et al. 2021), and are the basis of unWISE (Schlafly et al. 2019) and CatWISE2020 (Marocco et al. 2021) catalogues greatly improving over it. However, these catalogues still did not provide the detections or measurements for the objects at individual epochs.

In order to systematically search for cool rapidly moving objects in WISE data we used recently released unTimely catalogue (Meisner et al. 2023) which is the result of uniform analysis of individual epochal unWISE coadds (Meisner et al. 2019, 2018) using *crowdsourc* crowded-field photometry package (Schlafly et al. 2018; Schlafly 2021). It is currently distributed as a set of FITS tables each corresponding to the objects detected in one of two filters (W1 or W2) in individual epochal coadds for one of 18240 sky tiles. Typically every tile is covered with 15 to 17 unWISE coadds spanning approximately 11 years between Jan 2010 and Dec 2020 in every filter, but some of them (284 tiles, located close to ecliptic poles) have significantly more, up to two hundred, epochs spanning the same time interval (Meisner et al. 2018).

Epochal catalogues are independent, and not cross-matched together, both between different epoch and between different filters in a single epoch. Therefore, as we are primarily interested in detecting cool objects, we processed only the catalogues in W2 ($4.6\mu\text{m}$) band. Moreover, to ensure the consistency of depths of catalogues from individual epochs, we excluded from the analysis the epochs with total number of contributing exposures (`N_EXP` field in the unTimely metadata table) less than a half of the median value for that tile. We applied basic quality cuts to the objects from epochal catalogues by selecting only the detections from primary parts of unWISE coadds (`primary==1`) having flux measured with signal to noise ratio of at least 3. Additionally, we require the detections to have sufficiently large fraction of flux inside the PSF that comes from this object (`fracflux>0.5`) to ensure that the detections are not subject to significant crowding, and thus have reliable astrometry and (less relevant for us) photometry. After initial experimenting we decided not to perform any filtering on “quality factor” (`qf`) field or flags derived either from unWISE coadds themselves (`flags_unwise`) or from *crowdsourc* processing (`flags_info`) as they prevent most brighter objects from being detected, while not reducing significantly the amount of typical artefacts among the candidates.

2.1. Motion detection algorithm

After applying various quality cuts as described above we analyzed the sets of all objects from epochal catalogues for every tile in order to find candidate moving objects. To do so, we converted their sky coordinates to Cartesian ones on the unit sphere, and searched for linear structures in the resulting four-dimensional space (three spatial coordinates plus time). We used a simple “opportunistic” algorithm that consider all pairs of points from different epochs that satisfy the criteria of being separated by at least $6''$ (slightly more than 2 pixels in unWISE coadds, and slightly less than full-width at half maximum (FWHM) of its point-spread function (PSF)) but no more than $90''$ (for reducing the computational complexity), and not belonging to clusters containing more objects than half of number of epochs, within $1''$. The latter criterion helps filtering out stationary objects, while the former one ensures significant motion of the candidates, with both placing a lower limit on the detectable proper motion of about $0.6''/\text{year}^1$. We also excluded the pairs that contain the points already claimed by previously selected candidates – it helps uniquely identifying the candidate tracks by their first point, but, potentially, complicates the detection in too crowded fields. Then, for every pair, we formed a candidate track, computed its expected positions for all the epochs available for that tile, and then selected the objects from corresponding epochs (this time without applying any additional criteria on top of initial quality cuts) that are closer than $1''$ to these positions². We rejected the candidate tracks that do not have objects in more than 60% of the epochs, corresponding to at least 10 epochs in typical 16-epochal tile.

The candidates selected this way are prone to both genuine image-level artefacts, especially due to long spikes around bright stars, and spurious tracks formed from individual detections of stationary objects located approximately along a line. We could

¹ On the other hand, there is no practical upper limit on detectable proper motion as long as the track remains approximately linear.

² While this radius of $1''$ is significantly larger than typical positional uncertainties claimed in the catalogue we decided to adopt it and deal with spurious associations later on the trajectory fitting stage.

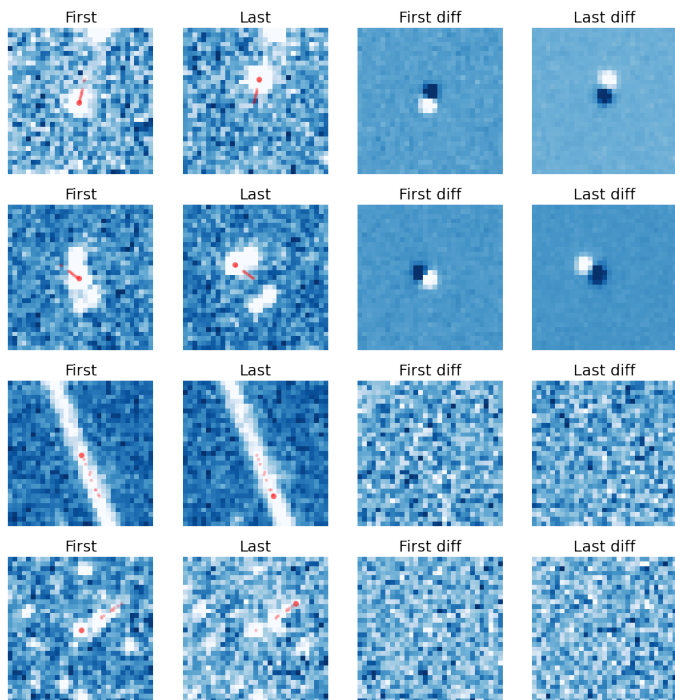


Fig. 1. Examples of images used to visually check the moving object candidates selected by the algorithm as described in Section 2.1. Each row displays the cutouts from the first and last epochs in unWISE coadds, and the corresponding differences between the images and median of all available epochs. All cutouts are centered on the position of the object from the first epoch (so that it is in the center in the first and third columns). Red dots mark the positions of the objects from all available epochs, with the larger circle corresponding to the current epoch of the image.

First and second rows display the actual moving objects, for an isolated and crowded fields, while the third one shows an artefact due to bright star spike, and the last – spurious candidate due to linking together individual detections of several stationary objects located roughly along the line.

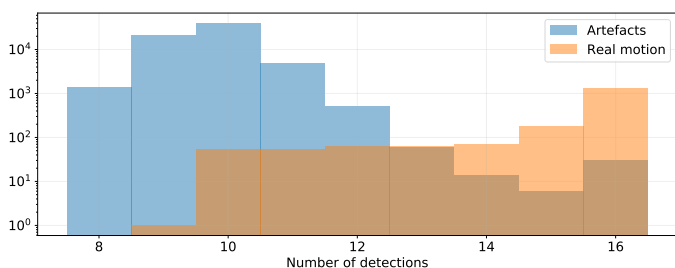


Fig. 2. Number of epochs where the object is visible for the artefacts and visually confirmed moving objects. Only the tiles with standard (15 to 17 epochs in total, 98.5% of all tiles) coverage are shown. Most but not all of spurious candidates are shorter than actual moving objects.

not find a way to reliably filter out either kind of artefacts using the information available in the catalogue files or positional residuals around the linear fit, and therefore visually checked all candidates with a simple dashboard based on the WISEView (Meisner et al. 2018; Caselden et al. 2018) cutout API developed in the frame of Backyard Worlds project (Kuchner et al. 2017). The dashboard displays, for every candidate, the cutouts from the first and last epochs at the object position, and the corresponding differences between these images and the median image of all epochs, and allows easy selection of real moving ob-

jects by the characteristic dipoles in the latter images, as shown in Figure 1. In the unclear cases, we also directly checked the epochal animations using the original WISEView web tool³.

This way, we selected 3245 candidates that passed visual inspection and thus reliably correspond to actual moving objects. Figure 2 shows the distribution of number of epochs where the object is detected, for both final candidates and artefacts. The amount of the latter significantly grows towards lower number of epochs, thus justifying limits on the selection parameters we used for the motion detection above, meaning that further releasing them is unpractical for this specific “opportunistic” algorithm.

2.2. Proper motions

For the final candidates that passed visual inspection we computed the proper motion by performing robust linear regression of their standard coordinates versus time using RANSAC (Fischler & Bolles 1981) algorithm as implemented in scikit-learn (Pedregosa et al. 2011) Python package in order to mitigate the influence of spurious associations of stationary objects with the track due to too permissive matching radius we used. Knowing proper motion, we then performed a cross-match with Gaia DR3 catalogue (Gaia Collaboration et al. 2023) by propagating object positions to its J2016.0 epoch, using 2'' matching radius, and only considering Gaia objects with significant proper motions to avoid confusions with faint stationary background stars. This way we found the associations for 2689 (82%) of all candidates. Left panel of Figure 3 shows that the agreement of proper motions is sufficiently good and unbiased for its whole range, while Figure 4 shows that the fraction of unassociated objects does not depend on the proper motion value, while slightly increasing for fainter fluxes⁴.

We also cross-matched the candidates with CatWISE2020 (Marocco et al. 2021) catalogue by propagating their positions to J2015.4 (MJD=57170) epoch, using catalogue columns corresponding to proper motion corrected positions for that epoch, and conservatively assuming 3'' (slightly more than unWISE coadds pixel size) matching radius. While we do find the associations for every candidate (see right panel of Figure 3), for significant part of them the association is not unique and contains, in addition to seemingly unbiased ones with comparable proper motions and fluxes, also the counterparts that are ~ 1 magnitude fainter and have $\sim 1''/\text{year}$ greater velocity. We attribute these spurious associations to systematic deblending problems in the catalogue introducing artificial detections.

We also checked for associated Simbad (Wenger et al. 2000) database entries for the candidates. As Simbad is highly heterogeneous and does not generally provide the epochs for the coordinates listed there, we, for every candidate, computed a number of trial positions propagated to the epochs from J1990.0 till J2021.0 with a step small enough to accommodate for candidate’s proper motion, and looked for Simbad entries within 5'' from these positions. This way we found the associations for all except 42 candidates, with none of them having Gaia DR3 counterpart. We additionally checked visually these 42 candidates in order to find potential problems with proper motion estimations or Simbad object displacements, and found none, thus conclud-

³ Available at <http://byw.tools/wisview>.

⁴ We should also note that some of unassociated objects, especially brighter ones, do actually have matching counterparts in either Gaia DR2 or Gaia eDR3 catalogues.

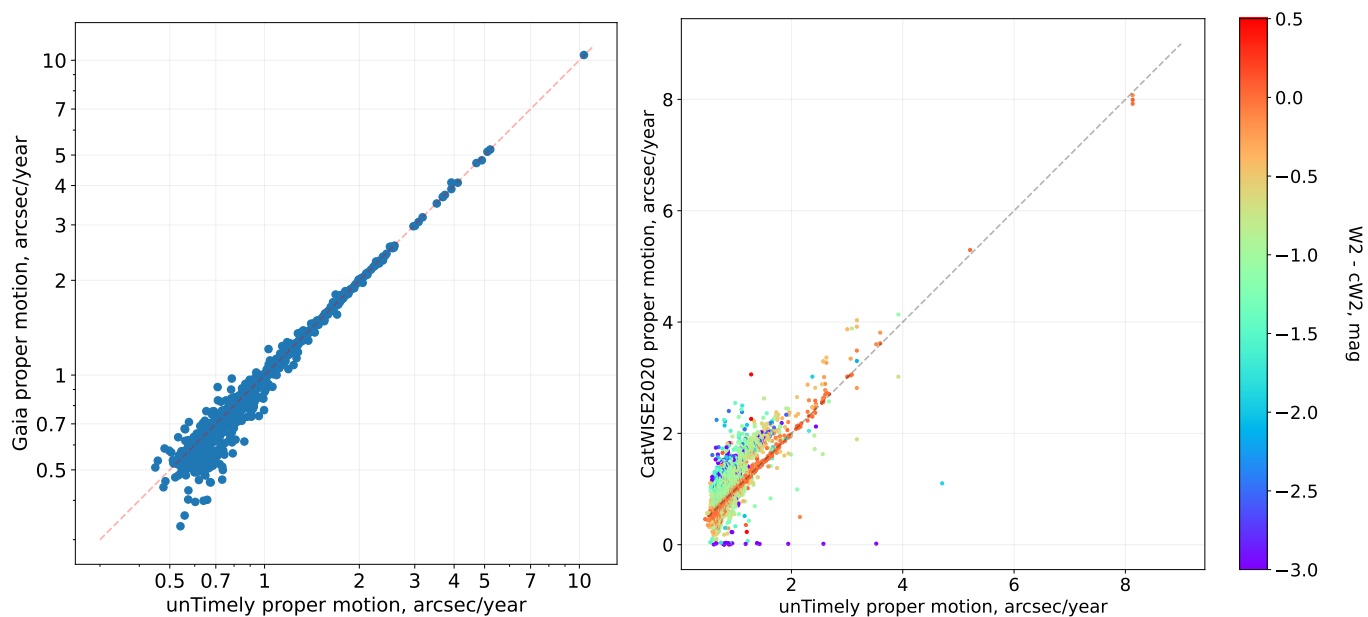


Fig. 3. Comparison of the proper motions measured in this work with values from Gaia DR3 (Gaia Collaboration et al. 2023) (left panel) and CatWISE2020 (Marocco et al. 2021) (right panel) catalogues. The latter panel also displays the difference between W2 band magnitudes in this work and the catalogue values. The agreement with Gaia proper motions is sufficiently good, with the spread increasing towards smaller values as the track length in unTimely data becomes too small to permit accurate measurement. On the other hand, CatWISE2020 contains, in addition to unbiased ones (red group along the diagonal line), a large number of spurious records matching with our objects but with systematically larger proper motions and fainter fluxes (by approximately 1 magnitude in a large number of cases), which we attribute to systematic deblending problems in the catalogue.

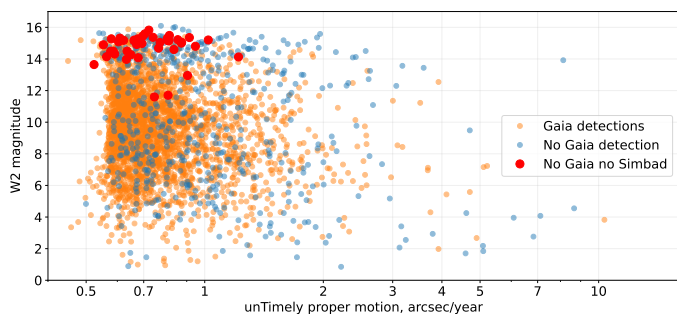


Fig. 4. Proper motion versus W2 magnitude for moving objects detected in this work and listed in Table 1. Colors designate the objects with and without Gaia DR3 associations, as well as the ones without associations with both Gaia DR3 and Simbad. As expected (see Section 2.1 for discussion of algorithm limitations), we systematically did not detect objects moving slower than approximately $0.5''/\text{year}$, or fainter than $W2 \sim 16.0$.

ing that these ones reliably lack Simbad records. We will discuss these in detail below in Section 3.1

3. Discussion

Table 1 shows the full list of high proper motion objects detected in our analysis, along with their Simbad associations. We successfully recovered the fastest known brown dwarf, WISEA J085510.74-071442.5 (Luhman 2014) (upper rightmost point in Figure 4 – note that CatWISE2020 contains three different objects associated to it, as seen in right panel of Figure 3), as well as the fastest known star, Barnard’s Star (lower rightmost point), but did not detect anything moving faster than that, despite the algorithm specifically being tailored for catching the largest proper motions.

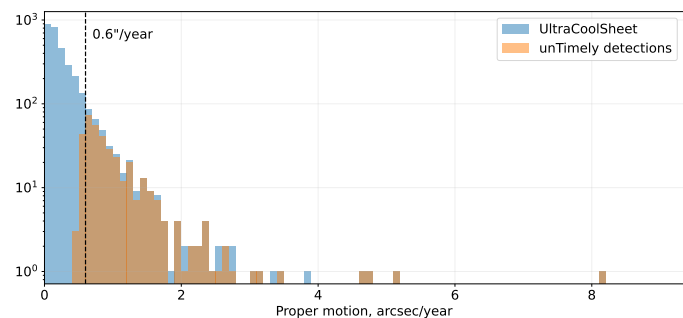


Fig. 5. Histogram of proper motions for known cool dwarfs from UltraCoolSheet (Best et al. 2024), along with its subset matched with the objects detected in our work. Proper motions are taken from the original UltraCoolSheet table, and therefore may slightly differ from the values measured in our work. As expected, the majority of objects faster than $\sim 0.6''/\text{year}$ are successfully identified in our analysis, with individual missing ones being either too faint to be detectable in epochal unTimely catalogues, or located in complicated sky regions with too few isolated detections.

In order to assess the sensitivity of the algorithm for detecting other known cool objects with high proper motions we cross-matched our detections with the list of known cool dwarfs from UltraCoolSheet (Best et al. 2024; Best et al. 2021, 2024) database. For that, we used CatWISE2020 positions from the database, and proceeded in the same way as we employed before. As it is seen in Figure 5, most of the objects moving faster than $\sim 0.6''/\text{year}$ are successfully detected in our analysis. We examined the data for several missing ones and found that they are either too faint to be detectable in epochal unTimely catalogues (in contrast e.g. to CatWISE2020 where detections are done in all-time coadded images which are significantly deeper), or situated in complicated fields with too few isolated detections.

3.1. Candidates without Simbad associations

Of all moving objects that we detected in our analysis, 42 are not listed in Simbad (Wenger et al. 2000) database, and thus may potentially be previously unknown brown dwarfs. To better assess them, we performed their association with several large catalogues both in infrared and optical range, by propagating their positions to the catalogue epoch where known. Specifically, we cross-matched the candidates with CatWISE2020 (Marocco et al. 2021), identified proper unique associations in ambiguous cases by comparing the brightness and proper motion (see Section 2.2 and right panel of Figure 3 for the discussion) and used their identifiers as a human-readable designation for the candidates from now on. We also cross-matched them with 2MASS point source catalogue (Skrutskie et al. 2006), the catalogue of Pan-STARRS DR2 epochal (“warp”) measurements (Chambers et al. 2016), VISTA Hemisphere Survey (McMahon et al. 2013), UKIRT Hemisphere Survey (Dye et al. 2018) epochal detections, SkyMapper DR4 (Onken et al. 2024) epochal detections, Sloan Digital Sky Survey DR16 (Ahumada et al. 2020), DENIS (Denis 2005), Dark Energy Survey DR2 (Abbott et al. 2021), and DELVE DR2 (Drlica-Wagner et al. 2022). In cases of ambiguous matches (especially for Dark Energy Survey which is based on a stack of multi-epoch images with no precise times specified) we inspected individual candidates and selected the ones with most compatible brightness values. For multi-epoch Pan-STARRS DR2, SkyMapper DR4, and DELVE DR2 data, with numerous separate detections of every object at different epochs, we assumed the median value for their magnitudes in every filter.

Despite detection of at least four of our candidates in Dark Energy Survey (see Table 3), none of them is in the list of ultracool dwarf candidates from DES 6-year data (dal Ponte et al. 2023), which is consistent with relatively large proper motions of our candidates. On the other hand, we also performed the search for these candidates in the UltraCoolSheet (Best et al. 2024; Best et al. 2021, 2024) compilative database of cool dwarfs⁵, and found two of them – CWISE J234627.27+665732.6 (#11) and CWISE J035532.23+474358.1 (#33) – there, originally published by Tinney et al. (2018) and (Smith et al. 2014), correspondingly. One more – CWISE J124909.08+362116.0 (#4) – was recently published by Burgasser et al. (2024) as an L subdwarf at the star/brown dwarf mass limit. Seven more candidates are also listed in Brooks et al. (2024). It supports the possibility of the other ones also being suitable candidates for brown dwarfs.

The summary of the data we assembled on the candidates is given in Table 2, and the full photometry is given in Table 3. Using these measurements, we constructed two-color diagrams⁶ that are shown in Figure 6, and overplotted the data for known cool dwarfs from Kirkpatrick et al. (2021) and UltraCoolSheet (Best et al. 2024) along with the template cool dwarfs colors from dal Ponte et al. (2023).

Right panel of Figure 6 shows that the spectral type for cool dwarfs is changing quite smoothly in the (K-W2) vs (J-

W2) plane. We may exploit it to make a simple estimation of the spectral types for the candidates, by taking a median type value in their vicinity there. For the candidates lacking J and K magnitudes but having the color $(W1-W2)>0.5$ we may use just it to also estimate the spectral type, albeit less reliably due to larger scatter. For $(W1-W2)<0.5$ the dependence of the type on the color is too weak to estimate it. Table 2 shows these tentative types estimated from either colors. In both cases, the spread of catalogue values in the candidate vicinity defines the range of possible candidate types. For the candidates having multi-color data in optical and near-infrared bands (see Table 3 and Table 4) we also used the VO SED Analyzer (VOSA⁷) (Bayo et al. 2008) to estimate the spectral type by template fitting, and got the results generally consistent with the ones we acquired from infrared colors.

In a similar manner, we may use the (W1-W2) vs absolute W2 magnitude plane (left panel of Figure 7) to estimate absolute magnitudes in W2 band for the candidates. To do so, for every candidate we selected all UltraCoolSheet objects falling within the 1σ range of its (W1-W2) with known parallaxes, and computed the median and median absolute deviation of their absolute magnitudes, to be used as an estimates for the candidate absolute magnitude and its uncertainty, correspondingly. Then, using these values, we estimated the distances to the candidates that are shown in right panel of Figure 7, and listed in Table 2. The projected velocities corresponding to observed proper motions and estimate distances, are shown in Figure 8.

3.2. Individual objects

CWISE J105716.29-675728.4 (#36) Association with this CatWISE2020 object is unreliable as it has inconsistent direction and amplitude of proper motion despite having consistent position and W2 magnitude. This is probably caused by a crowded field having several stationary objects around that confuse crowdsourcing pipeline. Therefore, we cannot fully believe in the magnitudes reported for this object in the catalogue, and thus computed them from unTimely epochal catalogues⁸ that give $(W1-W2)=-0.08\pm 0.06$. Together with optical and near-infrared colors, it suggests that the object is an early K-type star, with VOSA best fit corresponding to K2 type. Therefore we excluded this object from the spectral type analysis and distance estimation.

CWISE J140808.52-491759.4 (#39) has sufficiently large $(W1-W2)$ to be classified as T5, but its near-infrared (J and K) magnitudes place it among M9-L0 types in right panel of Figure 6. However, there is a known spectroscopically classified T4.5 dwarf CWISE J020743.00+000056.1 (Geballe et al. 2002) close to its position, so we may assume that the classification based on $(W1-W2)$ is correct for it.

⁷ VO SED Analyzer is available at <http://svo2.cab.inta-csic.es/svo/theory/vosa/>

⁸ For crowded fields like the one around CWISE J105716.29-675728.4, unTimely epochal magnitudes of individual objects often display prominent correlation of the magnitude with fracFlux parameter describing the fraction of the flux inside PSF footprint coming from the object itself. To account for it, we performed a linear fit of this dependency, and extrapolated it to $\text{fracFlux}=1$, i.e. fully uncrowded case, using the extrapolated value and its propagated error as magnitude estimation. As this procedure is not sufficiently stable, we did not perform similar fit for all other objects where CatWISE2020 associations are more reliable, using catalogue magnitudes instead.

⁵ UltraCoolSheet is available online at <http://bit.ly/UltracoolSheet>.

⁶ For WISE colors here and below we use CatWISE2020 values for both W1 and W2 bands, instead of deriving these quantities from unTimely catalogue. It is motivated both by complexity of combining measurements from different unTimely epochs with varying quality and degree of crowding, as well as by supposedly better accuracy of CatWISE values derived by a combined fit to all available images at once (Marocco et al. 2021). The only exception for that is CWISE J105716.29-675728.4 (#36) – see below.

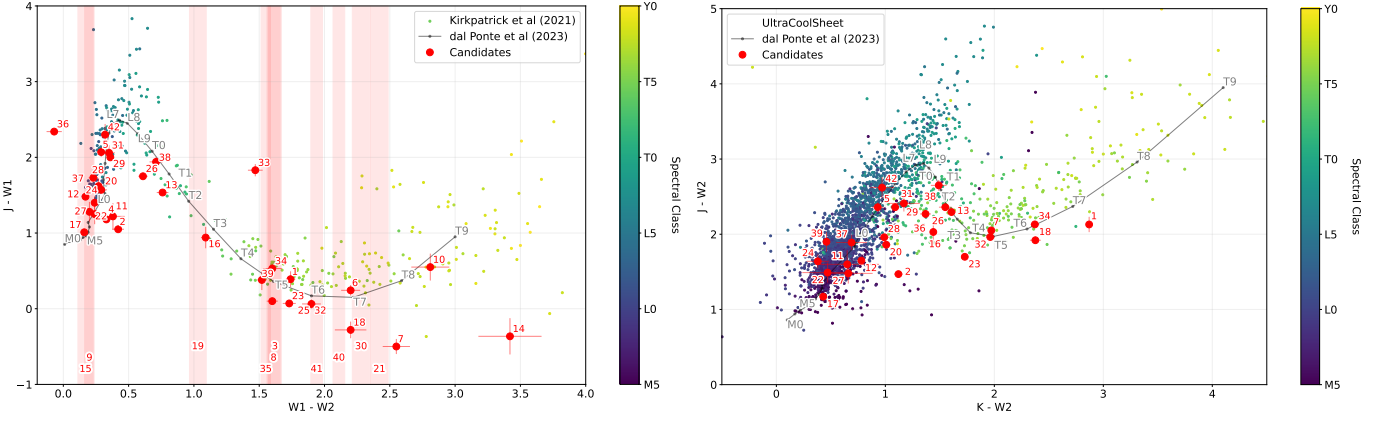


Fig. 6. Positions of the candidates from Table 2 (red circles) in two-color diagrams for the known brown dwarfs from Kirkpatrick et al. (2021) (left panel) and cool dwarfs from UltraCoolSheet (Best et al. 2024) (right panel). The colors of known objects correspond to their spectral class according to the color bars to the right of the plots. Red vertical bars represent the positions (with the width corresponding to 1σ error bars) of the candidates lacking the measurements in corresponding band. Black line marks the template colors of cool dwarfs according to dal Ponte et al. (2023). In these figures, we ignored minor differences between the passbands of different catalogues where near-infrared measurements are originated from (see Table 3 and Table 4), as they are typically negligible compared to the error bars of individual points.

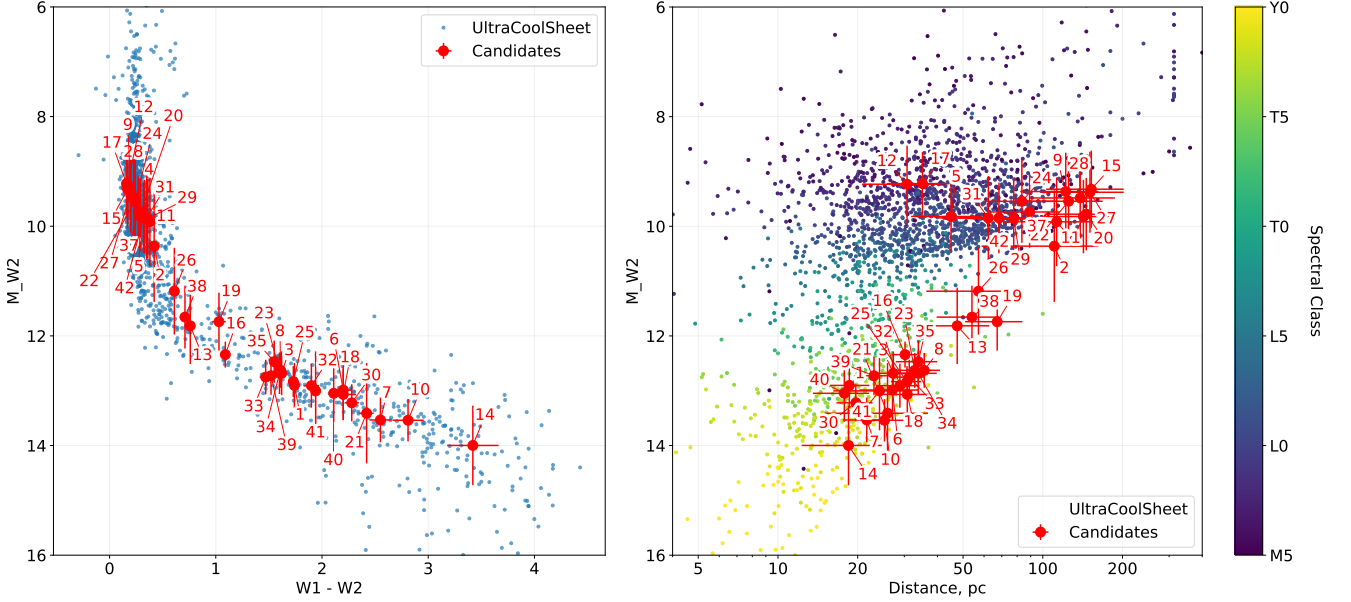


Fig. 7. Left panel – absolute W2 band magnitudes versus W1-W2 colors for cool dwarfs from UltraCoolSheet (Best et al. 2024) (blue dots), and the ones derived for the candidates from Table 2 (red circles) assuming they follow the same relation, as described in Section 3.2. Right panel – the distances to the candidates derived from these absolute magnitudes, along with the same for cool dwarfs from UltraCoolSheet. Lower right corner lacks objects as they are too faint to be detectable in WISE data.

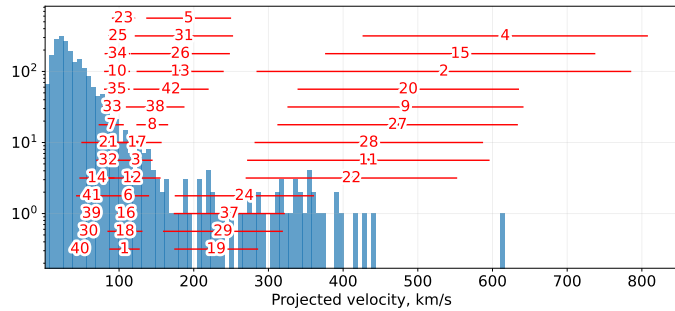


Fig. 8. Histogram of the projected velocities for cool dwarfs from UltraCoolSheet (Best et al. 2024) with known parallaxes and proper motions, and estimated ranges of projected velocity for the candidates from Table 2 (red horizontal bars).

CWISE J124909.08+362116.0 (#4) has $(W1-W2)=0.33$ and so its type cannot be reliably estimated from that color alone. VOSA template fitting of its multi-wavelength data gives best-fit L1 spectral type which is consistent with that color, and with the location of the object in Figure 6 and Figure 7. It is also consistent with sdL1 type derived from the spectrum by Burgasser et al. (2024).

CWISE J234627.27+665732.6 (#9) also has small $(W1-W2)=0.2$, but it lacks enough multi-wavelength measurements to achieve reasonable template fit with VOSA. Available data suggest late M or early L type.

CWISE J011128.00-103535.7 (#15) has $(W1-W2)=0.17$, VOSA template fit gives L0 spectral type for it.

CWISE J204928.79-443146.9 (#14) has T8-Y0 spectral type estimated from $(W1-W2)$ color that is consistent with T7.3 type previously published by Tinney et al. (2018).

CWISE J035532.23+474358.1 (#40) has T5-T7 spectral type estimated from $(W1-W2)$ colors that is consistent with T6 type previously published by Smith et al. (2014).

J230252.77-131458.0 (#18) is published in Brooks et al. (2024) with L1 spectral type at 142 ± 71 pc distance, but with very large χ^2 of the fit. Our estimation is T4–T5 based on $(W1-W2)$ color, and T4.5 based on VOSA fit, and the distance is 31 ± 7 pc. Moreover, our direct estimation of proper motion is nearly twice as large as CatWISE2020 value employed by Brooks et al. (2024). Therefore, we tend to believe in our estimations, and consider the object reliable T-dwarf candidate.

J104222.34-834921.2 (#22) is published in Brooks et al. (2024) with M8 spectral type, consistent with our estimation of M7–M9.

J110048.87-554006.8 (#24) is published in Brooks et al. (2024) with M9 spectral type, consistent with our estimation of M6–L1.

J060302.31+321532.1 (#27) is published in Brooks et al. (2024) with M8 spectral type, consistent with our estimation of M7–M9.

J194428.05+053344.8 (#31) is published in Brooks et al. (2024) with M4 spectral type. Our estimation is M9–T3 based on $(K-W2)-(J-W2)$ colors, and L6 based on VOSA fit.

J220134.02-041609.5 (#32) is published in Brooks et al. (2024) with L1 spectral type, but with very large χ^2 of the fit. Our estimation is T4–T6 based on $(K-W2)-(J-W2)$ colors, and T6.5 based on VOSA fit. Thus, we again consider our estimation correct, and consider the object a reliable T dwarf candidate.

J093016.98+604631.2 (#41) is published in Brooks et al. (2024) with T6 spectral type, consistent with our estimation of T5–T7. We consider it a reliable T dwarf candidate.

Reliable brown dwarf candidates. Based on the positions in Figure 6 and Figure 7 and estimated spectral types we may conclude that at least the following 15 objects, in addition to previously published ones mentioned above, are also reliable late-type brown dwarf candidates that should be targets for more detailed investigation: CWISE J053046.20+440849.2 (#1), CWISE J062316.19+071505.6 (#3), CWISE J105018.24-683054.9 (#6), CWISE J214706.01-540407.6 (#7), CWISE J011816.64-723917.9 (#8), CWISE J140048.92+253759.8 (#10), CWISE J075744.48-300504.3 (#16), CWISE J045456.23-742522.6 (#21), CWISE J024641.43-634329.2 (#23),

CWISE J095855.00+540305.4 (#25), CWISE J092710.37-474155.5 (#30), CWISE J102332.99+221527.6 (#33), CWISE J141403.72-171531.1 (#34), CWISE J184526.47+754829.7 (#35), CWISE J140808.52-491759.4 (#39), All of them have estimated distances closer than 50 pc and types later than T0.

4. Conclusions

We performed a systematic search for the objects with high proper motions in W2 band WISE data using recently released unTimely epochal catalogue, and successfully identified 3245 objects moving faster than $0.6''/\text{year}$. Our estimations of their proper motions are in a good agreement with Gaia DR3 measurements where they are available. We did not detect any object moving faster than approx. $10''/\text{year}$, but were able to successfully recover both the fastest-moving known brown dwarf WISEA J085510.74-071442.5 and most of other known rapidly moving normal stars and nearby cool dwarfs. We also identified 42 objects that do not have associated records in Simbad database, 32 of them not previously published. We assembled multi-wavelength information for them by cross-matching their trajectories with large optical and infrared catalogues, and used their colors to estimate their spectral types, distances and projected velocities. At least 15 of them are reliable brown dwarf candidates with estimated distances closer than 50 pc and types later than T0.

Acknowledgements. This work was co-funded by the EU and supported by the Czech Ministry of Education, Youth and Sports through the project CZ.02.01.01/00/22_008/0004596. This research was partially funded by the Ministry of Science and Higher Education of the Russian Federation, according to the research project 13.2251.21.0177 (075-15-2022-1228). This work has benefited from The UltracoolSheet at <http://bit.ly/UltracoolSheet>, maintained by Will Best, Trent Dupuy, Michael Liu, Aniket Sanghi, Rob Siverd, and Zhoujian Zhang, and developed from compilations by Dupuy & Liu (2012, ApJS, 201, 19), Dupuy & Kraus (2013, Science, 341, 1492), Deacon et al. (2014, ApJ, 792, 119), Liu et al. (2016, ApJ, 833, 96), Best et al. (2018, ApJS, 234, 1), Best et al. (2021, AJ, 161, 42), Sanghi et al. (2023, ApJ, 959, 63), and Schneider et al. (2023, AJ, 166, 103). This publication makes use of VOSA, developed under the Spanish Virtual Observatory (<https://svo.cab.inta-csic.es>) project funded by MCIN/AEI/10.13039/501100011033/ through grant PID2020-112949GB-I00. VOSA has been partially updated by using funding from the European Union's Horizon 2020 Research and Innovation Programme, under Grant Agreement No 776403 (EXOPLANETS-A)

References

- Abbott, T. M. C., Adamów, M., Agüena, M., et al. 2021, ApJS, 255, 20
 Ahumada, R., Allende Prieto, C., Almeida, A., et al. 2020, ApJS, 249, 3
 Bayo, A., Rodrigo, C., Barrado Y Navascués, D., et al. 2008, A&A, 492, 277
 Best, W. M. J., Dupuy, T. J., Liu, M. C., et al. 2024, The UltracoolSheet: Photometry, Astrometry, Spectroscopy, and Multiplicity for 4000+ Ultracool Dwarfs and Imaged Exoplanets
 Best, W. M. J., Liu, M. C., Magnier, E. A., et al. 2015, ApJ, 814, 118
 Best, W. M. J., Liu, M. C., Magnier, E. A., & Dupuy, T. J. 2021, AJ, 161, 42
 Best, W. M. J., Magnier, E. A., Liu, M. C., et al. 2018, ApJS, 234, 1
 Best, W. M. J., Sanghi, A., Liu, M. C., Magnier, E. A., & Dupuy, T. J. 2024, ApJ, 967, 115
 Brooks, H., Caselden, D., Kirkpatrick, J. D., et al. 2024, arXiv e-prints, arXiv:2408.14447
 Burgasser, A. J., Gerasimov, R., Kremer, K., et al. 2024, arXiv e-prints, arXiv:2407.08578
 Burningham, B., Cardoso, C. V., Smith, L., et al. 2013, MNRAS, 433, 457
 Carnero Rosell, A., Santiago, B., dal Ponte, M., et al. 2019, MNRAS, 489, 5301
 Caselden, D., Westin, Paul, L., Meisner, A., Kuchner, M., & Colin, G. 2018, WISEView: Visualizing motion and variability of faint WISE sources, Astrophysics Source Code Library, record ascl:1806.004
 Chambers, K. C., Magnier, E. A., Metcalfe, N., et al. 2016, arXiv e-prints, arXiv:1612.05560
 Chiu, K., Fan, X., Leggett, S. K., et al. 2006, AJ, 131, 2722

Table 1. High proper motion objects detected in this work. Only first 40 records, and a subset of columns, are shown, while the complete table is available online.

Unique ID	RA	Dec	Epoch MJD	pmRA arcsec/year	pmDec arcsec/year	W2 mag	pm arcsec/year	pm Gaia arcsec/year	Simbad
2688p045w2o0025372e001	269.4495	4.7242	55456	-0.62 ± 0.05	10.32 ± 0.02	3.83 ± 0.00	10.34	10.39	Barnard's star
0788m455w2o0028019e000	77.9449	-45.0345	55249	6.51 ± 0.06	-5.71 ± 0.02	4.55 ± 0.00	8.66	—	HD 33793
1342m076w2o0027045e001	133.7953	-7.2451	55321	-8.10 ± 0.05	0.66 ± 0.02	13.92 ± 0.04	8.13	—	WISEA J085510.74-071442.5
1781p378w2o00111596e000	178.2595	37.7020	55344	4.00 ± 0.01	-5.88 ± 0.03	4.08 ± 0.00	7.11	—	HD 103095
3469m364w2o0023991e000	346.4911	-35.8491	55340	6.71 ± 0.05	1.28 ± 0.02	2.76 ± 0.00	6.83	—	HD 217987
0018m379w2o0026788e000	1.3724	-37.3641	55352	5.62 ± 0.04	-2.33 ± 0.01	3.96 ± 0.00	6.09	—	HD 225213
1225p090w2o0009243e000	122.9930	8.7585	55303	1.06 ± 0.01	-5.10 ± 0.01	7.23 ± 0.00	5.21	5.21	Ross 619
0440p166w2o0017388e000	43.2638	16.8706	55228	3.42 ± 0.02	-3.79 ± 0.01	7.16 ± 0.00	5.10	5.12	Teegarden's Star b
3174p393w2o0004832e000	316.7405	38.7589	55347	4.02 ± 0.03	3.13 ± 0.03	1.84 ± 0.00	5.09	—	* 61 Cyg A
3174p393w2o0004657e000	316.7456	38.7514	55347	4.03 ± 0.04	3.10 ± 0.03	2.18 ± 0.00	5.09	—	* 61 Cyg B
1660p363w2o0007263e000	165.8324	35.9562	55335	-0.58 ± 0.01	-4.86 ± 0.02	2.67 ± 0.00	4.90	4.81	[ZEH2003] RX J1103.3+3559.2
1647p075w2o0003990e000	164.1092	7.0070	55346	-3.85 ± 0.03	-2.71 ± 0.06	5.58 ± 0.00	4.71	4.72	Wolf 359
3323m576w2o0029882e000	331.0651	-56.7899	55318	3.98 ± 0.02	-2.51 ± 0.00	9.48 ± 0.00	4.71	—	* eps Ind B
1664p439w2o0006206e001	166.3509	43.5296	55524	-4.50 ± 0.04	1.02 ± 0.06	4.25 ± 0.00	4.61	—	BD+44 2051
3295m576w2o0026103e002	330.8694	-56.7959	56779	3.72 ± 0.09	-2.70 ± 0.06	1.70 ± 0.00	4.59	—	* eps Ind
0640m076w2o0011226e002	63.8308	-7.6690	56705	-2.07 ± 0.06	-3.55 ± 0.06	5.43 ± 0.00	4.11	4.08	* omi02 Eri C
2042p030w2o0024100e000	204.1223	3.6764	55210	-3.76 ± 0.01	-1.13 ± 0.01	12.54 ± 0.01	3.92	3.90	Wolf 489
0640m076w2o0011262e002	63.8090	-7.6663	56705	-2.01 ± 0.09	-3.37 ± 0.03	1.98 ± 0.00	3.92	4.09	* omi02 Eri b
0178p545w2o0029817e000	17.0849	54.9158	55222	3.46 ± 0.03	-1.55 ± 0.02	2.94 ± 0.00	3.79	—	* mu. Cas
1124p045w2o0033512e000	111.8539	5.2153	55294	0.46 ± 0.04	-3.71 ± 0.01	4.30 ± 0.00	3.74	3.74	BD+05 1668
2279m167w2o0018036e000	227.5511	-16.4729	55237	-1.02 ± 0.01	-3.54 ± 0.02	7.12 ± 0.00	3.69	3.68	HD 134440
2279m167w2o0019629e000	227.5516	-16.3893	55237	-1.00 ± 0.02	-3.54 ± 0.02	6.96 ± 0.00	3.68	3.68	HD 134439
2671p832w2o0006516e000	267.4266	82.7833	55273	-1.43 ± 0.01	3.30 ± 0.01	13.44 ± 0.01	3.60	—	EGGR 199
2208m197w2o0002522e000	221.0761	-20.3292	55230	-2.92 ± 0.00	-1.97 ± 0.01	11.22 ± 0.00	3.52	3.51	SSSPM J1444-2019
3193m394w2o0023066e001	319.3007	-38.8709	55497	-3.05 ± 0.07	-1.08 ± 0.03	2.55 ± 0.00	3.24	—	V* AX Mic
1744p666w2o0027744e000	175.0866	67.2500	55317	0.25 ± 0.01	-3.17 ± 0.00	8.43 ± 0.00	3.18	3.17	Ross 451
2492m682w2o0003788e000	249.9201	-68.7940	55265	0.58 ± 0.02	-3.12 ± 0.01	13.57 ± 0.02	3.17	—	WISE J163940.83-684738.6
0041p439w2o0017537e002	4.6074	44.0241	55571	3.11 ± 0.07	0.52 ± 0.03	3.41 ± 0.00	3.15	—	HD 1326c
0505m425w2o0002411e000	49.9934	-43.0678	55211	3.04 ± 0.05	0.72 ± 0.03	2.07 ± 0.00	3.12	—	* e Eri
0540m122w2o0024847e000	54.5695	-11.4946	55230	1.47 ± 0.00	-2.71 ± 0.01	8.54 ± 0.00	3.08	3.07	Ross 578
1683m258w2o0004191e000	168.7034	-26.3077	55364	-3.04 ± 0.01	-0.38 ± 0.01	12.30 ± 0.01	3.06	—	2MASS J11145133-2618235
0121p060w2o0001682e000	12.2948	5.3807	55383	1.24 ± 0.01	-2.74 ± 0.00	11.36 ± 0.00	3.00	2.98	Wolf 28
2897m455w2o0014661e000	290.2025	-45.5665	55291	0.71 ± 0.03	-2.89 ± 0.02	6.52 ± 0.00	2.97	2.97	L 347-14
1712p651w2o0031078e000	169.9995	65.8469	55317	-2.95 ± 0.02	0.14 ± 0.02	5.17 ± 0.00	2.95	—	V* SZ UMa
1627m531w2o0012782e000	162.3154	-53.3185	55205	-2.79 ± 0.03	0.40 ± 0.03	7.35 ± 0.00	2.82	—	Luhman 16
1747m652w2o0030973e000	176.4464	-64.8425	55224	2.65 ± 0.01	-0.33 ± 0.01	11.09 ± 0.00	2.67	—	LAWD 37
0812p832w2o0005622e000	83.2730	82.7745	55268	2.03 ± 0.00	-1.67 ± 0.01	13.25 ± 0.01	2.63	—	2MASS J05325346+8246465
2807m637w2o0010334e000	281.2887	-63.9615	55282	2.55 ± 0.02	0.60 ± 0.01	7.85 ± 0.00	2.62	—	SCR J1845-6357
0438p030w2o0002613e000	43.5394	2.3996	55223	2.60 ± 0.01	0.21 ± 0.01	12.72 ± 0.01	2.61	—	2MASS J02540788+0223563
3432m061w2o000958e000	343.4797	-6.7837	55350	2.49 ± 0.01	-0.72 ± 0.01	13.25 ± 0.02	2.59	2.58	EGGR 453

Notes.

- (¹) Unique ID corresponds to `unwise_detid` field of the first detection of the object in unTimely epochal catalogues.
(²) C coordinates and epoch here correspond to predicted position of the object at the time of first detection. (³) W 2 magnitudes and errors are computed as simple averages of corresponding epochal values, without any additional filtering.
(⁴) P proper motion of the closest Gaia DR3 match.
(⁵) F first identifier for a closest matching object from Simbad. See the text for details on how exactly the association is performed.

- Cutri, R. M., Wright, E. L., Conrow, T., et al. 2021, *VizieR Online Data Catalog: AllWISE Data Release (Cutri+ 2013)*, *VizieR On-line Data Catalog: II/328*. Originally published in: IPAC/Caltech (2013)
- dal Ponte, M., Santiago, B., Carnero Rosell, A., et al. 2023, *MNRAS*, 522, 1951
- Day-Jones, A. C., Marocco, F., Pinfield, D. J., et al. 2013, *MNRAS*, 430, 1171
- Delfosse, X., Tinney, C. G., Forveille, T., et al. 1997, *A&A*, 327, L25
- Delorme, P., Delfosse, X., Albert, L., et al. 2008, *A&A*, 482, 961
- Denis, C. 2005, *VizieR Online Data Catalog: The DENIS database (DENIS Consortium, 2005)*, *VizieR On-line Data Catalog: B/denis*. Originally published in: The DENIS consortium (2005)
- Drlica-Wagner, A., Ferguson, P. S., Adamów, M., et al. 2022, *ApJS*, 261, 38
- Dye, S., Lawrence, A., Read, M. A., et al. 2018, *MNRAS*, 473, 5113
- Fan, X., Knapp, G. R., Strauss, M. A., et al. 2000, *AJ*, 119, 928
- Fischler, M. A. & Bolles, R. C. 1981, *Commun. ACM*, 24, 381–395
- Gaia Collaboration, Vallenari, A., Brown, A. G. A., et al. 2023, *A&A*, 674, A1
- Geballe, T. R., Knapp, G. R., Leggett, S. K., et al. 2002, *ApJ*, 564, 466
- Hayashi, C. & Nakano, T. 1963, *Progress of Theoretical Physics*, 30, 460
- Kirkpatrick, J. D., Cushing, M. C., Gelino, C. R., et al. 2011, *ApJS*, 197, 19
- Kirkpatrick, J. D., Gelino, C. R., Faherty, J. K., et al. 2021, *ApJS*, 253, 7
- Kirkpatrick, J. D., Looper, D. L., Burgasser, A. J., et al. 2010, *ApJS*, 190, 100
- Kirkpatrick, J. D., Reid, I. N., Liebert, J., et al. 1999, *The Astrophysical Journal*, 519, 802
- Kirkpatrick, J. D., Schneider, A., Fajardo-Acosta, S., et al. 2014, *ApJ*, 783, 122
- Kuchner, M. J., Faherty, J. K., Schneider, A. C., et al. 2017, *ApJ*, 841, L19
- Kumar, S. S. 1963, *The Astrophysical Journal*, 137, 1121
- Lodieu, N., Pérez-Garrido, A., Béjar, V. J. S., et al. 2014, *Astronomy and Astrophysics*, 569, A120
- Luhman, K. L. 2014, *ApJ*, 786, L18
- Marocco, F., Eisenhardt, P. R. M., Fowler, J. W., et al. 2021, *ApJS*, 253, 8
- Marocco, F., Kirkpatrick, J. D., Schneider, A. C., et al. 2024, *ApJ*, 967, 147
- McMahon, R. G., Banerji, M., Gonzalez, E., et al. 2013, *The Messenger*, 154, 35
- Meisner, A. M., Caselden, D., Schlafly, E. F., & Kiwy, F. 2023, *AJ*, 165, 36
- Meisner, A. M., Lang, D., Schlafly, E. F., & Schlegel, D. J. 2019, *PASP*, 131, 124504
- Meisner, A. M., Lang, D., & Schlegel, D. J. 2018, *AJ*, 156, 69
- Mužić, K., Schödel, R., Scholz, A., et al. 2017, *Monthly Notices of the Royal Astronomical Society*, 471, 3699
- Nakajima, T., Oppenheimer, B. R., Kulkarni, S. R., et al. 1995, *Nature*, 378, 463
- Onken, C. A., Wolf, C., Bessell, M. S., et al. 2024, *arXiv e-prints*, arXiv:2402.02015
- Pedregosa, F., Varoquaux, G., Gramfort, A., et al. 2011, *Journal of Machine Learning Research*, 12, 2825
- Phan-Bao, N., Bessell, M. S., Martín, E. L., et al. 2008, *MNRAS*, 383, 831
- Rebolo, R., Zapatero Osorio, M. R., & Martín, E. L. 1995, *Nature*, 377, 129
- Rothermich, A., Faherty, J. K., Bardalez-Gagliuffi, D., et al. 2024, *AJ*, 167, 253
- Schlafly, E. F. 2021, *crowdsourc: Crowded field photometry pipeline*, *Astrophysics Source Code Library*, record ascl:2106.004
- Schlafly, E. F., Green, G. M., Lang, D., et al. 2018, *ApJS*, 234, 39
- Schlafly, E. F., Meisner, A. M., & Green, G. M. 2019, *ApJS*, 240, 30
- Schmidt, S. J., West, A. A., Hawley, S. L., & Pineda, J. S. 2010, *AJ*, 139, 1808
- Skrutskie, M. F., Cutri, R. M., Stiening, R., et al. 2006, *AJ*, 131, 1163
- Smith, L., Lucas, P. W., Bunce, R., et al. 2014, *MNRAS*, 443, 2327
- Tinney, C. G., Kirkpatrick, J. D., Faherty, J. K., et al. 2018, *ApJS*, 236, 28
- Wenger, M., Ochsenein, F., Egret, D., et al. 2000, *A&AS*, 143, 9
- Wright, E. L., Eisenhardt, P. R. M., Mainzer, A. K., et al. 2010, *AJ*, 140, 1868

Table 2. Summary information for the candidates lacking both Gaia DR2 and Simbad counterparts.

	CWISE	RA J2016.0	Dec J2016.0	pm "/year	W2	M_W2	SpT	Distance pc	V _{tan} km/s	
1	J053046.20+440849.2	82.6924	44.1473	1.22 ± 0.03	14.25 ± 0.02	12.90 ± 0.41	T0–T8 ¹²	19 ± 4	107 ± 20	
2	J011552.59+454814.1	18.9688	-45.8040	1.02 ± 0.07	15.58 ± 0.04	10.36 ± 1.02	M8–L1 ¹²	111 ± 52	535 ± 251	
3	J062316.19+071505.6	95.8174	7.2516	0.95 ± 0.03	14.86 ± 0.03	12.68 ± 0.40	T4–T6 ¹³	27 ± 5	122 ± 23	
4	J124909.08+362116.0	192.2880	36.3548	0.91 ± 0.07	15.59 ± 0.06	9.82 ± 0.67	L1 ¹⁴	142 ± 44	617 ± 191	(1)
5	J171342.26+443112.5	258.4262	-44.5201	0.90 ± 0.02	13.09 ± 0.02	9.82 ± 0.64	L0–L6 ¹²	45 ± 13	193 ± 57	
6	J105018.24+683054.9	162.5774	-68.5153	0.87 ± 0.07	15.15 ± 0.02	12.99 ± 0.54	T6–T7 ¹³	27 ± 7	112 ± 28	
7	J214706.01+540407.6	326.7740	-54.0688	0.87 ± 0.05	15.21 ± 0.03	13.53 ± 0.41	T4–T6 ¹²	22 ± 4	89 ± 17	
8	J011816.64+723917.9	19.5654	-72.6550	0.85 ± 0.04	15.39 ± 0.03	12.63 ± 0.32	T4–T6 ¹³	36 ± 5	144 ± 21	
9	J234627.27+665732.6	356.6121	66.9591	0.84 ± 0.04	14.80 ± 0.03	9.37 ± 0.71		122 ± 40	483 ± 158	
10	J140048.92+253759.8	210.2038	25.6333	0.81 ± 0.05	15.55 ± 0.04	13.54 ± 0.39	T7–T9 ¹³	25 ± 5	97 ± 17	
11	J224250.43+132837.7	340.7102	-13.4775	0.81 ± 0.07	15.18 ± 0.08	9.92 ± 0.81	M8–L0 ¹²	113 ± 42	434 ± 162	
12	J065233.95+223046.8	103.1414	22.5131	0.81 ± 0.03	11.67 ± 0.01	9.23 ± 0.70	M9–L1 ¹²	31 ± 10	118 ± 38	
13	J211250.11+052925.2	318.2090	-5.4902	0.81 ± 0.05	15.20 ± 0.04	11.82 ± 0.70	T2–T4 ¹²	48 ± 15	182 ± 58	
14	J204928.79+443146.9	312.3697	-44.5298	0.80 ± 0.09	15.33 ± 0.03	14.00 ± 0.73	T8–Y0 ¹³	18 ± 6	70 ± 24	(2)
15	J011128.00+103535.7	17.8664	-10.5930	0.77 ± 0.04	15.24 ± 0.05	9.32 ± 0.70	L0 ¹⁴	153 ± 50	557 ± 181	
16	J075744.48+300504.3	119.4353	-30.0846	0.76 ± 0.03	14.74 ± 0.03	12.34 ± 0.24	T3–T5 ¹²	30 ± 3	109 ± 12	
17	J141946.85+610910.3	214.9464	-61.1527	0.75 ± 0.03	11.95 ± 0.01	9.22 ± 0.58	M5–M7 ¹²	35 ± 9	124 ± 33	
18	J230252.77+131458.0	345.7199	-13.2494	0.74 ± 0.05	15.51 ± 0.05	13.07 ± 0.47	T4–T5 ¹²	31 ± 7	108 ± 23	(3)
19	J114557.19+673327.5	176.4898	67.5577	0.72 ± 0.05	15.88 ± 0.05	11.74 ± 0.53	T2–T4 ¹³	67 ± 16	230 ± 56	
20	J021059.50+395414.2	32.7480	-39.9040	0.70 ± 0.04	15.60 ± 0.04	9.78 ± 0.66	M8–L4 ¹²	146 ± 44	487 ± 148	
21	J045456.23+742522.6	73.7352	-74.4229	0.70 ± 0.02	15.48 ± 0.03	13.41 ± 0.92	T7–T8 ¹³	26 ± 11	86 ± 36	
22	J104222.34+834921.2	160.6012	-83.8227	0.69 ± 0.03	15.03 ± 0.03	9.54 ± 0.75	M7–M9 ¹²	125 ± 43	411 ± 142	(4)
23	J024641.43+634329.2	41.6714	-63.7248	0.68 ± 0.03	15.21 ± 0.03	12.63 ± 0.32	T4–T5 ¹²	33 ± 5	106 ± 16	
24	J110048.87+554006.8	165.2038	-55.6685	0.68 ± 0.02	14.15 ± 0.02	9.54 ± 0.76	M6–L1 ¹²	83 ± 29	268 ± 93	(5)
25	J095855.00+540305.4	149.7298	54.0515	0.68 ± 0.03	15.27 ± 0.03	12.83 ± 0.28	T5–T6 ¹³	31 ± 4	98 ± 13	
26	J222721.75+325119.5	336.8402	32.8554	0.67 ± 0.03	14.97 ± 0.03	11.18 ± 0.79	T2–T3 ¹²	57 ± 21	182 ± 66	
27	J060302.31+321532.1	90.7595	32.2589	0.66 ± 0.04	15.27 ± 0.04	9.38 ± 0.74	M7–M9 ¹²	151 ± 51	473 ± 161	(6)
28	J201029.81+015100.3	302.6243	1.8501	0.66 ± 0.07	15.19 ± 0.03	9.48 ± 0.76	M9–L5 ¹²	138 ± 49	434 ± 153	
29	J210819.58+182318.3	317.0814	18.3884	0.65 ± 0.02	14.31 ± 0.02	9.86 ± 0.73	L0–L7 ¹²	78 ± 26	239 ± 80	
30	J092710.37+474155.5	141.7937	-47.6986	0.64 ± 0.04	14.69 ± 0.03	13.22 ± 0.34	T6–T8 ¹³	20 ± 3	59 ± 9	
31	J194428.05+053344.8	296.1168	5.5622	0.63 ± 0.02	13.82 ± 0.04	9.85 ± 0.76	M9–T3 ¹²	62 ± 22	187 ± 66	(7)
32	J220134.02+041609.5	330.3919	-4.2694	0.62 ± 0.04	15.21 ± 0.04	12.91 ± 0.40	T4–T6 ¹²	29 ± 5	85 ± 16	(8)
33	J102332.99+221527.6	155.8875	22.2577	0.61 ± 0.06	15.23 ± 0.04	12.75 ± 0.31	T4–T6 ¹³	31 ± 5	91 ± 13	
34	J141403.72+171531.1	213.5154	-17.2588	0.61 ± 0.03	15.33 ± 0.04	12.68 ± 0.38	T4–T6 ¹²	34 ± 6	98 ± 17	
35	J184526.47+754829.7	281.3607	75.8084	0.60 ± 0.02	15.12 ± 0.02	12.47 ± 0.39	T4–T5 ¹³	34 ± 6	97 ± 17	
36	J105716.29+675728.4	164.3176	-67.9571	0.59 ± 0.03	13.86 ± 0.05		K2 ¹⁴			(9)
37	J010803.06+204741.1	17.0127	-20.7948	0.59 ± 0.03	14.49 ± 0.02	9.74 ± 0.65	M9–L1 ¹²	89 ± 27	248 ± 74	
38	J065919.42+161551.8	104.8309	16.2643	0.58 ± 0.04	15.32 ± 0.04	11.66 ± 0.57	T0–T3 ¹²	54 ± 14	148 ± 39	
39	J140808.52+491759.4	212.0358	-49.3000	0.58 ± 0.03	14.54 ± 0.02	12.73 ± 0.35	T5 ¹³	23 ± 4	63 ± 10	
40	J035532.23+474358.1	58.8838	47.7328	0.56 ± 0.03	14.30 ± 0.02	13.05 ± 0.52	T5–T7 ¹³	18 ± 4	48 ± 11	(10)
41	J093016.98+604631.2	142.5714	60.7754	0.55 ± 0.03	14.92 ± 0.02	13.00 ± 0.72	T5–T7 ¹³	24 ± 8	63 ± 21	(11)
42	J062158.80+220048.5	95.4951	22.0131	0.52 ± 0.03	14.02 ± 0.02	9.85 ± 0.64	L1–L6 ¹²	68 ± 20	170 ± 50	

Notes.

(1) P ublished in Burgasser et al. (2024) as an sdL1 subdwarf with $0.884 \pm 0.005''/\text{year}$ proper motion at 125 ± 8 pc distance having 103 ± 10 km/s radial velocity.

(2) P ublished in Tinney et al. (2018) with estimated T7.3 spectral type, and included in UltraCoolSheet (Best et al. 2024).

(3) P ublished in Brooks et al. (2024) with L1 spectral type and 142 ± 71 pc distance. See Section 3.2 for more detailed discussion.

(4) P ublished in Brooks et al. (2024) with M8 spectral type and 126 ± 1 pc distance.

(5) P ublished in Brooks et al. (2024) with M9 spectral type and 77 pc distance.

(6) P ublished in Brooks et al. (2024) with M8 spectral type and 138 ± 17 pc distance.

(7) P ublished in Brooks et al. (2024) with M4 spectral type and 509 ± 102 pc distance.

(8) P ublished in Brooks et al. (2024) with L1 spectral type and 174 ± 44 pc distance. See Section 3.2 for more detailed discussion.

(9) C atWISE2020 association unreliable. WISE magnitudes computed from unTimely measurements. Optical and IR colors consistent with early K-type star.

(10) P ublished in Smith et al. (2014) with estimated T6 spectral type at approximately 19 pc distance, and included in UltraCoolSheet (Best et al. 2024).

(11) P ublished in Brooks et al. (2024) with T6 spectral type and 23 ± 1 pc distance.

(12) S pectral type estimated from the position in (K-W2) - (J-W2) plane.

(13) S pectral type estimated from (W1-W2) color.

(14) S pectral type estimated from VOSA (Bayo et al. 2008) template fitting of multi-wavelength measurements.

Table 3. Photometric information for the candidates lacking both Gaia DR2 and Simbad counterparts, collected from several large-scale catalogues, both optical and infrared. Identifiers from corresponding catalogues are listed, when available (they are excluded for multi-epochal detections from UKIRT Hemisphere Survey).

	CWISE	cW1	cW2	2MASS	J	H	K
1	J053046.20+440849.2	15.99±0.03	14.25±0.02	05304606+4409108	16.38±0.1	16.14±0.18	17.12
2	J011552.59-454814.1	16.0±0.02	15.58±0.04				
3	J062316.19+071505.6	16.48±0.04	14.86±0.03				
4	J124909.08+362116.0	15.92±0.03	15.59±0.06				
5	J171342.26-443112.5	13.38±0.02	13.09±0.02	17134270-4430582	15.45±0.06	14.65±0.06	14.02±0.05
6	J105018.24-683054.9	17.35±0.07	15.15±0.02				
7	J214706.01-540407.6	17.76±0.1	15.21±0.03				
8	J011816.64-723917.9	17.0±0.04	15.39±0.03				
9	J234627.27+665732.6	15.0±0.02	14.8±0.03				
10	J140048.92+253759.8	18.36±0.14	15.55±0.04				
11	J224250.43-132837.7	15.56±0.04	15.18±0.08	22424980-1328327	16.78±0.17	16.13±0.21	15.83±0.28
12	J065233.95+223046.8	11.84±0.01	11.67±0.01	06523341+2231022	13.32±0.02	12.83±0.02	12.45±0.02
13	J211250.11-052925.2	15.96±0.02	15.2±0.04				
14	J204928.79-443146.9	18.75±0.24	15.33±0.03				
15	J011128.00-103535.7	15.41±0.03	15.24±0.05				
16	J075744.48-300504.3	15.83±0.02	14.74±0.03	07574409-3004522	16.77±0.14	15.66	16.18
17	J141946.85-610910.3	12.11±0.02	11.95±0.01	14194814-6109061	13.12±0.03	12.6±0.03	12.38±0.03
18	J230252.77-131458.0	17.71±0.11	15.51±0.05				
19	J114557.19+673327.5	16.91±0.04	15.88±0.05				
20	J021059.50-395414.2	15.89±0.02	15.6±0.04				
21	J045456.23-742522.6	17.9±0.06	15.48±0.03				
22	J104222.34-834921.2	15.27±0.03	15.03±0.03	10422782-8349283	16.52±0.13	15.94±0.16	15.5±0.23
23	J024641.43-634329.2	16.81±0.03	15.21±0.03				
24	J110048.87-554006.8	14.39±0.02	14.15±0.02	11004991-5540085	15.79±0.09	15.06±0.08	14.53±0.1
25	J095855.00+540305.4	17.0±0.04	15.27±0.03				
26	J222721.75+325119.5	15.58±0.02	14.97±0.03				
27	J060302.31+321532.1	15.47±0.02	15.27±0.04	06030167+3215406	16.75±0.13	16.21±0.18	15.93±0.22
28	J201029.81+015100.3	15.42±0.02	15.19±0.03				
29	J210819.58+182318.3	14.67±0.02	14.31±0.02				
30	J092710.37-474155.5	16.97±0.06	14.69±0.03				
31	J194428.05+053344.8	14.17±0.02	13.82±0.04	19442837+0533519	16.23±0.1	15.45±0.11	14.99±0.14
32	J220134.02-041609.5	17.11±0.06	15.21±0.04				
33	J102332.99+221527.6	16.7±0.04	15.23±0.04				
34	J141403.72-171531.1	16.93±0.06	15.33±0.04				
35	J184526.47+754829.7	16.67±0.03	15.12±0.02				
36	J105716.29-675728.4	13.79±0.03	13.86±0.05				
37	J010803.06-204741.1	14.76±0.02	14.49±0.02	01080249-2047363	16.38±0.1	15.79±0.14	15.18±0.14
38	J065919.42+161551.8	16.03±0.03	15.32±0.04				
39	J140808.52-491759.4	16.06±0.03	14.54±0.02	14080921-4917538	16.44±0.13	15.46	15.0
40	J035532.23+474358.1	16.41±0.04	14.3±0.02				
41	J093016.98+604631.2	16.86±0.04	14.92±0.02				
42	J062158.80+220048.5	14.34±0.02	14.02±0.02	06215882+2200540	16.64±0.14	15.81±0.15	14.99±0.11

	VHS	Y	J	H	Ks	UHS	J	K
1							16.07±0.01	16.54±0.06
2	J011552.35-454811.0		17.05	16.95	16.7			
4							17.1±0.03	
6	J105018.15-683054.8		17.5931					
7	J214705.54-540405.2		17.261	17.5703	17.1821			
10							18.91±0.11	
11	J224250.37-132836.9	17.3844	16.4725		16.1947			
12							13.22	12.42
13	J211250.31-052921.7	18.6425	17.4953	16.9838	16.8068			
14	J204928.67-443145.3		18.3856					
18	J230252.75-131456.3	18.6651	17.4302		17.8866			
20	J021059.55-395412.9		17.4605		16.6081			
22	J104222.73-834921.8		16.5881		15.803			
23	J024641.20-634329.6		16.9101		16.9388			
25							17.07±0.02	
26							17.33±0.03	16.52±0.05
28							17.15±0.03	16.18±0.04
29							16.67±0.02	15.4±0.02
31							16.23±0.01	14.82±0.01
32	J220133.87-041611.3	18.3676	17.1731	17.5335	17.1726			
33							18.53±0.07	
34	J141403.82-171530.6	18.6006	17.4613		17.702			
36	J105716.01-675726.4		16.13		15.2291			
38							17.97±0.06	16.81±0.06
39	J140808.72-491758.2		16.2442		16.4099			

Table 4. Photometric information for the candidates lacking both Gaia DR2 and Simbad counterparts, collected from several large-scale catalogues, both optical and infrared. Identifiers from corresponding catalogues are listed, when available (they are excluded for multi-epochal detections from Pan-STARRS, SkyMapper DR4, and DELVE DR2).

	Pan-STARRS DR2	r	i	z	y	DENIS	I	J	K
1				20.2±0.1	18.77±0.09				
3					19.99±0.19				
4			21.69±0.16	20.01±0.07	18.97±0.13				
5						J171342.6-443058		15.26±0.16	
9				20.51±0.22	19.43±0.14				
11			20.54±0.16	18.92±0.04	18.14±0.06				
12		19.39±0.03	16.68±0.01	15.35	14.77±0.01				
13				20.69±0.15	19.53±0.17				
15			21.11±0.11	19.59±0.12	18.58±0.06				
17						J141948.1-610906	14.26±0.04	13.08±0.08	12.26±0.1
18					20.09±0.14				
24						J110049.9-554008	17.53±0.12	15.84±0.17	
25				21.21±0.21	19.88±0.14				
26				20.66±0.16	19.44±0.14				
27			21.15±0.12	19.43±0.04	18.51±0.05				
28			20.08±0.05	20.23±0.12	19.22±0.12				
29				19.83±0.05	18.78±0.08				
31			21.22±0.11	19.35±0.05	18.37±0.05				
32				21.16±0.18					
34					20.13±0.1				
35				21.19±0.2	19.34±0.18				
37			21.17±0.13	19.37±0.05	18.3±0.05				
38				21.19±0.21	19.97±0.17				
40					19.21±0.09				
41					19.7±0.22				
42			20.51±0.05	19.56±0.07	18.67±0.06				

	DES DR2	g	r	i	z	y
2	J011552.47-454812.7	24.0±0.16	22.85±0.08	21.36±0.04	19.93±0.02	19.34±0.04
7	J214706.08-540408.4			24.6±0.48	21.64±0.06	20.66±0.07
14	J204928.85-443147.7				22.55±0.16	21.26±0.18
23	J024641.43-634329.0	24.17±0.18	24.07±0.22	23.16±0.17	20.56±0.03	19.6±0.05
37	J010803.09-204741.4		23.26±0.08	20.59±0.01	18.76±0.01	18.27±0.01

	SkyMapper DR4	g	r	i	z	SDSS DR16	i	z
2	1617769695				19.25±0.2			
3						J062316.17+071513.7		20.81±0.14
4						J124908.75+362127.2	21.84±0.14	19.7±0.07
5	356470723			19.09±0.31	17.95±0.1			
11	6156455				18.5±0.05			
13						J211250.38-052920.7		20.06±0.16
15	1018117938				18.92±0.03			
17		16.8±0.04	14.76±0.02	15.82±0.05	14.36±0.06			
22					18.56±0.17			
24	418966254				18.68±0.02			
25						J095855.80+540310.0		20.61±0.18
26						J222721.38+325118.9		20.1±0.11
36		18.08±0.1	17.33±0.19	16.91±0.43	16.43±0.45			
37	12308530				18.82±0.03			

	DELVE DR2	g	r	i	z
8		23.95±0.09	23.3±0.09	23.01±0.09	20.9±0.07
15			23.07±0.12	20.61±0.02	18.97±0.01
18					21.16±0.05
20			23.85±0.25	21.94±0.06	20.0±0.02
22			23.39±0.11	20.1±0.02	18.69±0.01
23				23.05±0.23	20.6±0.03
26					20.05±0.02
32					20.91±0.04
33					22.46±0.15
37			23.08±0.08	20.57±0.02	18.75±0.01
39				23.24±0.13	19.66±0.01